

J. L. WILLIS,¹³³ B. WILLKE,^{17,8} M. H. WIMMER,^{8,17} W. WINKLER,⁸ C. C. WIPF,¹ H. WITTEL,^{8,17} G. WOAN,³⁶ J. WORDEN,³⁷
 J. L. WRIGHT,³⁶ G. WU,⁶ J. YABLON,⁸² W. YAM,¹⁰ H. YAMAMOTO,¹ C. C. YANCEY,⁶² M. J. YAP,²⁰ H. YU,¹⁰ M. YVERT,⁷
 A. ZADROŻNY,¹¹⁰ L. ZANGRANDO,⁴² M. ZANOLIN,⁹⁷ J.-P. ZENDRI,⁴² M. ZEVIN,⁸² F. ZHANG,¹⁰ L. ZHANG,¹ M. ZHANG,¹¹⁹
 Y. ZHANG,¹¹² C. ZHAO,⁵¹ M. ZHOU,⁸² Z. ZHOU,⁸² X. J. ZHU,⁵¹ M. E. ZUCKER,^{1,10} S. E. ZURAW,¹⁰¹ AND J. ZWEIZIG¹

†Deceased, May 2015. ‡Deceased, March 2015.

(LIGO Scientific Collaboration and Virgo Collaboration)

- ¹LIGO, California Institute of Technology, Pasadena, CA 91125, USA
²Louisiana State University, Baton Rouge, LA 70803, USA
³Università di Salerno, Fisciano, I-84084 Salerno, Italy
⁴INFN, Sezione di Napoli, Complesso Universitario di Monte S. Angelo, I-80126 Napoli, Italy
⁵University of Florida, Gainesville, FL 32611, USA
⁶LIGO Livingston Observatory, Livingston, LA 70754, USA
⁷Laboratoire d'Annecy-le-Vieux de Physique des Particules (LAPP), Université Savoie Mont Blanc, CNRS/IN2P3, F-74941 Annecy-le-Vieux, France
⁸Albert-Einstein-Institut, Max-Planck-Institut für Gravitationsphysik, D-30167 Hannover, Germany
⁹Nikhef, Science Park, 1098 XG Amsterdam, Netherlands
¹⁰LIGO, Massachusetts Institute of Technology, Cambridge, MA 02139, USA
¹¹Instituto Nacional de Pesquisas Espaciais, 12227-010 São José dos Campos, São Paulo, Brazil
¹²INFN, Gran Sasso Science Institute, I-67100 L'Aquila, Italy
¹³INFN, Sezione di Roma Tor Vergata, I-00133 Roma, Italy
¹⁴Inter-University Centre for Astronomy and Astrophysics, Pune 411007, India
¹⁵International Centre for Theoretical Sciences, Tata Institute of Fundamental Research, Bangalore 560012, India
¹⁶University of Wisconsin-Milwaukee, Milwaukee, WI 53201, USA
¹⁷Leibniz Universität Hannover, D-30167 Hannover, Germany
¹⁸Università di Pisa, I-56127 Pisa, Italy
¹⁹INFN, Sezione di Pisa, I-56127 Pisa, Italy
²⁰Australian National University, Canberra, Australian Capital Territory 0200, Australia
²¹The University of Mississippi, University, MS 38677, USA
²²California State University Fullerton, Fullerton, CA 92831, USA
²³LAL, Université Paris-Sud, CNRS/IN2P3, Université Paris-Saclay, 91400 Orsay, France
²⁴Chennai Mathematical Institute, Chennai 603103, India
²⁵Università di Roma Tor Vergata, I-00133 Roma, Italy
²⁶University of Southampton, Southampton SO17 1BJ, United Kingdom
²⁷Universität Hamburg, D-22761 Hamburg, Germany
²⁸INFN, Sezione di Roma, I-00185 Roma, Italy
²⁹Albert-Einstein-Institut, Max-Planck-Institut für Gravitationsphysik, D-14476 Potsdam-Golm, Germany
³⁰APC, AstroParticule et Cosmologie, Université Paris Diderot, CNRS/IN2P3, CEA/Irfu, Observatoire de Paris, Sorbonne Paris Cité, F-75205 Paris Cedex 13, France
³¹Montana State University, Bozeman, MT 59717, USA
³²Università di Perugia, I-06123 Perugia, Italy
³³INFN, Sezione di Perugia, I-06123 Perugia, Italy
³⁴European Gravitational Observatory (EGO), I-56021 Cascina, Pisa, Italy
³⁵Syracuse University, Syracuse, NY 13244, USA
³⁶SUPA, University of Glasgow, Glasgow G12 8QQ, United Kingdom
³⁷LIGO Hanford Observatory, Richland, WA 99352, USA
³⁸Wigner RCP, RMKI, H-1121 Budapest, Konkoly Thege Miklós út 29-33, Hungary
³⁹Columbia University, New York, NY 10027, USA
⁴⁰Stanford University, Stanford, CA 94305, USA
⁴¹Università di Padova, Dipartimento di Fisica e Astronomia, I-35131 Padova, Italy
⁴²INFN, Sezione di Padova, I-35131 Padova, Italy
⁴³CAMK-PAN, 00-716 Warsaw, Poland
⁴⁴Astronomical Observatory Warsaw University, 00-478 Warsaw, Poland

- ⁴⁵University of Birmingham, Birmingham B15 2TT, United Kingdom
- ⁴⁶Università degli Studi di Genova, I-16146 Genova, Italy
- ⁴⁷INFN, Sezione di Genova, I-16146 Genova, Italy
- ⁴⁸RRCAT, Indore MP 452013, India
- ⁴⁹Faculty of Physics, Lomonosov Moscow State University, Moscow 119991, Russia
- ⁵⁰SUPA, University of the West of Scotland, Paisley PA1 2BE, United Kingdom
- ⁵¹University of Western Australia, Crawley, Western Australia 6009, Australia
- ⁵²Department of Astrophysics/IMAPP, Radboud University Nijmegen, P.O. Box 9010, 6500 GL Nijmegen, Netherlands
- ⁵³Artemis, Université Côte d’Azur, CNRS, Observatoire Côte d’Azur, CS 34229, Nice cedex 4, France
- ⁵⁴MTA Eötvös University, “Lendulet” Astrophysics Research Group, Budapest 1117, Hungary
- ⁵⁵Institut de Physique de Rennes, CNRS, Université de Rennes 1, F-35042 Rennes, France
- ⁵⁶Washington State University, Pullman, WA 99164, USA
- ⁵⁷Università degli Studi di Urbino “Carlo Bo,” I-61029 Urbino, Italy
- ⁵⁸INFN, Sezione di Firenze, I-50019 Sesto Fiorentino, Firenze, Italy
- ⁵⁹University of Oregon, Eugene, OR 97403, USA
- ⁶⁰Laboratoire Kastler Brossel, UPMC-Sorbonne Universités, CNRS, ENS-PSL Research University, Collège de France, F-75005 Paris, France
- ⁶¹VU University Amsterdam, 1081 HV Amsterdam, Netherlands
- ⁶²University of Maryland, College Park, MD 20742, USA
- ⁶³Center for Relativistic Astrophysics and School of Physics, Georgia Institute of Technology, Atlanta, GA 30332, USA
- ⁶⁴Institut Lumière Matière, Université de Lyon, Université Claude Bernard Lyon 1, UMR CNRS 5306, 69622 Villeurbanne, France
- ⁶⁵Laboratoire des Matériaux Avancés (LMA), IN2P3/CNRS, Université de Lyon, F-69622 Villeurbanne, Lyon, France
- ⁶⁶Universitat de les Illes Balears, IAC3—IEEC, E-07122 Palma de Mallorca, Spain
- ⁶⁷Università di Napoli “Federico II,” Complesso Universitario di Monte S. Angelo, I-80126 Napoli, Italy
- ⁶⁸NASA/Goddard Space Flight Center, Greenbelt, MD 20771, USA
- ⁶⁹Canadian Institute for Theoretical Astrophysics, University of Toronto, Toronto, Ontario M5S 3H8, Canada
- ⁷⁰Tsinghua University, Beijing 100084, China
- ⁷¹Texas Tech University, Lubbock, TX 79409, USA
- ⁷²The Pennsylvania State University, University Park, PA 16802, USA
- ⁷³National Tsing Hua University, Hsinchu City, 30013 Taiwan, Republic of China
- ⁷⁴Charles Sturt University, Wagga Wagga, New South Wales 2678, Australia
- ⁷⁵University of Chicago, Chicago, IL 60637, USA
- ⁷⁶Caltech CaRT, Pasadena, CA 91125, USA
- ⁷⁷Korea Institute of Science and Technology Information, Daejeon 305-806, Korea
- ⁷⁸Carleton College, Northfield, MN 55057, USA
- ⁷⁹Università di Roma “La Sapienza,” I-00185 Roma, Italy
- ⁸⁰University of Brussels, Brussels 1050, Belgium
- ⁸¹Sonoma State University, Rohnert Park, CA 94928, USA
- ⁸²Northwestern University, Evanston, IL 60208, USA
- ⁸³University of Minnesota, Minneapolis, MN 55455, USA
- ⁸⁴The University of Melbourne, Parkville, Victoria 3010, Australia
- ⁸⁵The University of Texas Rio Grande Valley, Brownsville, TX 78520, USA
- ⁸⁶The University of Sheffield, Sheffield S10 2TN, United Kingdom
- ⁸⁷University of Sannio at Benevento, I-82100 Benevento, Italy and INFN, Sezione di Napoli, I-80100 Napoli, Italy
- ⁸⁸Montclair State University, Montclair, NJ 07043, USA
- ⁸⁹Università di Trento, Dipartimento di Fisica, I-38123 Povo, Trento, Italy
- ⁹⁰INFN, Trento Institute for Fundamental Physics and Applications, I-38123 Povo, Trento, Italy
- ⁹¹Cardiff University, Cardiff CF24 3AA, United Kingdom
- ⁹²National Astronomical Observatory of Japan, 2-21-1 Osawa, Mitaka, Tokyo 181-8588, Japan
- ⁹³School of Mathematics, University of Edinburgh, Edinburgh EH9 3FD, United Kingdom
- ⁹⁴Indian Institute of Technology, Gandhinagar Ahmedabad Gujarat 382424, India
- ⁹⁵Institute for Plasma Research, Bhat, Gandhinagar 382428, India

- ⁹⁶University of Szeged, Dóm tér 9, Szeged 6720, Hungary
- ⁹⁷Embry-Riddle Aeronautical University, Prescott, AZ 86301, USA
- ⁹⁸University of Michigan, Ann Arbor, MI 48109, USA
- ⁹⁹Tata Institute of Fundamental Research, Mumbai 400005, India
- ¹⁰⁰American University, Washington, D.C. 20016, USA
- ¹⁰¹University of Massachusetts-Amherst, Amherst, MA 01003, USA
- ¹⁰²University of Adelaide, Adelaide, South Australia 5005, Australia
- ¹⁰³West Virginia University, Morgantown, WV 26506, USA
- ¹⁰⁴University of Białystok, 15-424 Białystok, Poland
- ¹⁰⁵SUPA, University of Strathclyde, Glasgow G1 1XQ, United Kingdom
- ¹⁰⁶IISER-TVM, CET Campus, Trivandrum Kerala 695016, India
- ¹⁰⁷Institute of Applied Physics, Nizhny Novgorod, 603950, Russia
- ¹⁰⁸Pusan National University, Busan 609-735, Korea
- ¹⁰⁹Hanyang University, Seoul 133-791, Korea
- ¹¹⁰NCBJ, 05-400 Świerk-Otwock, Poland
- ¹¹¹IM-PAN, 00-956 Warsaw, Poland
- ¹¹²Rochester Institute of Technology, Rochester, NY 14623, USA
- ¹¹³Monash University, Victoria 3800, Australia
- ¹¹⁴Seoul National University, Seoul 151-742, Korea
- ¹¹⁵University of Alabama in Huntsville, Huntsville, AL 35899, USA
- ¹¹⁶ESPCI, CNRS, F-75005 Paris, France
- ¹¹⁷Università di Camerino, Dipartimento di Fisica, I-62032 Camerino, Italy
- ¹¹⁸Southern University and A&M College, Baton Rouge, LA 70813, USA
- ¹¹⁹College of William and Mary, Williamsburg, VA 23187, USA
- ¹²⁰Instituto de Física Teórica, University Estadual Paulista/ICTP South American Institute for Fundamental Research, São Paulo SP 01140-070, Brazil
- ¹²¹University of Cambridge, Cambridge CB2 1TN, United Kingdom
- ¹²²IISER-Kolkata, Mohanpur, West Bengal 741252, India
- ¹²³Rutherford Appleton Laboratory, HSIC, Chilton, Didcot, Oxon OX11 0QX, United Kingdom
- ¹²⁴Whitman College, 345 Boyer Avenue, Walla Walla, WA 99362 USA
- ¹²⁵National Institute for Mathematical Sciences, Daejeon 305-390, Korea
- ¹²⁶Hobart and William Smith Colleges, Geneva, NY 14456, USA
- ¹²⁷Janusz Gil Institute of Astronomy, University of Zielona Góra, 65-265 Zielona Góra, Poland
- ¹²⁸Andrews University, Berrien Springs, MI 49104, USA
- ¹²⁹Università di Siena, I-53100 Siena, Italy
- ¹³⁰Trinity University, San Antonio, TX 78212, USA
- ¹³¹University of Washington, Seattle, WA 98195, USA
- ¹³²Kenyon College, Gambier, OH 43022, USA
- ¹³³Abilene Christian University, Abilene, TX 79699, USA

ABSTRACT

A transient gravitational-wave signal was identified in the twin Advanced LIGO detectors on September 14, 2015 at 09:50:45 UTC (GW150914). To assess the implications of this discovery, the detectors remained in operation with unchanged configurations over a period of 39 d around the time of the signal. A search of 16 days of simultaneous two-detector observational data found GW150914 to have a false alarm probability (FAP) of $< 2 \times 10^{-7}$. Parameter estimation followup on this trigger identifies its source as a binary black hole (BBH) merger with component masses $(m_1, m_2) = (36_{-4}^{+5}, 29_{-4}^{+4}) M_\odot$ at redshift $z = 0.09_{-0.04}^{+0.03}$. Here we report on the constraints these observations place on the rate of BBH coalescences. Considering only GW150914, assuming that all BBHs in the universe have the same masses and spins as this event, imposing a false alarm threshold of 1 per 100 years, and assuming that the BBH merger rate is constant in the comoving frame, we infer a 90% credible range of $2\text{--}53 \text{ Gpc}^{-3} \text{ yr}^{-1}$ (comoving frame). Incorporating all triggers that pass the search threshold while

accounting for the uncertainty in the astrophysical origin of each trigger, we estimate a higher rate, ranging from 6–400 $\text{Gpc}^{-3} \text{yr}^{-1}$ depending on assumptions about the BBH mass distribution. All together, our various rate estimates fall in the conservative range 2–400 $\text{Gpc}^{-3} \text{yr}^{-1}$.

1. INTRODUCTION

The first detection of a gravitational wave (GW) signal in the twin Advanced LIGO detectors on September 14, 2015, 09:50:45 UTC was reported in [Abbott et al. \(2016a\)](#). This transient signal is designated GW150914. In a search of 16 days of two-detector data for signals from mergers of compact binary systems, the false alarm rate (FAR) of GW150914 is less than $4.9 \times 10^{-6} \text{yr}^{-1}$, for a false alarm probability (FAP) of $< 2 \times 10^{-7}$. GW150914 is consistent with a gravitational-wave signal from the merger of two black holes with masses $(m_1, m_2) = (36_{-4}^{+5}, 29_{-4}^{+4}) M_{\odot}$ at redshift $z = 0.09_{-0.04}^{+0.03}$ ([Abbott et al. 2016e](#)). In this paper, we discuss inferences on the rate of binary black hole (BBH) mergers from this detection and the surrounding data.

Previous estimates of the BBH merger rate based on electromagnetic observations and analytic population modeling are reviewed in [Abadie et al. \(2010\)](#). The range of rates given spans more than three orders of magnitude, from 0.1–300 $\text{Gpc}^{-3} \text{yr}^{-1}$. The rate of BBH mergers is a crucial output from BBH population models (see, for example, [Kalogera et al. 2007](#); [Dominik et al. 2012](#); [Spera et al. 2015](#)), but uncertainty about the theory of the evolution of massive stellar binaries and a lack of constraining electromagnetic observations produces a wide range of rate estimates. Observations of GWs can tightly constrain this rate with minimal modeling assumptions, and thus provide useful input on the astrophysics of massive stellar binaries. In the absence of detections until GW150914, the most constraining rate upper-limits from GW observations, as detailed in [Aasi et al. \(2013\)](#), lie above the modeled range. Here, for the first time, we report on GW observations that constrain the model space of BBH merger rates.

It is possible to obtain a rough estimate of the BBH coalescence rate from the GW150914 detection by setting a low FAR threshold that eliminates other search triggers ([Abbott et al. 2016d](#)). The inferred rate will depend on the detector sensitivity to the BBH population, which strongly depends on BBH masses. However, our single detection leaves a large uncertainty in the mass distribution of merging BBH systems. [Kim et al. \(2003\)](#) faced a similar situation in deriving binary neutron star merger rates from the small sample of Galactic double neutron star systems. They argued that an approach assuming each detected system belongs to its own class, deriving merger rates for each class independently, and then adding the rates over classes to infer the overall merger rate gives a good estimate. If we follow [Kim](#)

[et al. \(2003\)](#), assume that all BBH mergers in the universe have the same source-frame masses and spins as GW150914, and set a nominal threshold on the FAR of one per century, then the inferred posterior median rate and 90% credible range is $R_{100} = 14_{-12}^{+39} \text{Gpc}^{-3} \text{yr}^{-1}$ (see [Section 2.2](#)).

Merger rates inferred from a single trigger that is so much more significant than any other trigger are sensitive to the choice of threshold. Less significant search triggers with FAR above one per century can also provide information about the merger rate. For example, the second most significant trigger in the search had a FAR of 0.43yr^{-1} (FAP 0.02). Under the assumption that it is astrophysical in origin, parameter estimation (PE) ([Veitch et al. 2015](#)) indicates that its source is a BBH merger with source-frame masses $(m_1, m_2) = (23_{-5}^{+18}, 13_{-5}^{+4}) M_{\odot}$ at redshift $z = 0.2_{-0.1}^{+0.1}$. Triggers like this have $\sim 2\%$ chance of arising from noise within the 16 days of coincident observations and, therefore, cannot be confidently claimed as detections. Indeed, we show in [Section 2.1](#) that, based on two different searches, with different models for the rates at which both noise triggers and astrophysical signals appear in the LIGO detectors, we find posterior probabilities 0.84 and 0.91 that LVT151012 is of astrophysical origin; this is the only other trigger from either search that has probability greater than 50% of being of astrophysical origin. [Farr et al. \(2015\)](#) presented a method by which a set of triggers of uncertain origin like this can be used to produce a rate estimate that is more accurate than that produced by considering only highly significant events.

Incorporating our uncertainty about the astrophysical origin of all search triggers that could represent BBH signals ([Abbott et al. 2016d](#)) following [Farr et al. \(2015\)](#), assuming that the BBH merger rate is constant in comoving volume and source-frame time, and making various assumptions about the mass distribution of merging BBH systems as described in [Sections 2.2](#) and [3](#), we derive merger rates that lie in the range 6–400 $\text{Gpc}^{-3} \text{yr}^{-1}$.

Our rate estimates are summarized in [Table 1](#); see [Section 2.2](#) for more information. Each row of [Table 1](#) represents a different assumption about the BBH mass distribution. The first two columns giving rates correspond to different search methods with different models of the astrophysical and terrestrial trigger distributions. Because the estimates from the different searches are consistent with each other, the third column giving rates provides a combined estimate that results from an average of the posterior densities from each search. All num-

Table 1. Rates of BBH mergers estimated under various assumptions. See Section 2.2.

Mass Distribution	$R/(\text{Gpc}^{-3}\text{yr}^{-1})$		
	pycbc	gstlal	Combined
GW150914	16_{-13}^{+38}	17_{-14}^{+39}	17_{-13}^{+39}
LVT151012	61_{-53}^{+152}	62_{-55}^{+164}	62_{-54}^{+165}
Both	82_{-61}^{+155}	84_{-64}^{+172}	83_{-63}^{+168}
Astrophysical			
Flat	33_{-26}^{+64}	32_{-25}^{+65}	33_{-26}^{+62}
Power Law	102_{-79}^{+198}	99_{-79}^{+203}	100_{-79}^{+201}

bers are quoted as a posterior median with a symmetric 90% credible range. All together, our rate estimates lie in the conservative range $2\text{--}400\text{ Gpc}^{-3}\text{yr}^{-1}$.

All our rate estimates are consistent within their statistical uncertainties, and these estimates are also consistent with the broad range of rate predictions reviewed in [Abadie et al. \(2010\)](#) with only the low end ($< 1\text{ Gpc}^{-3}\text{yr}^{-1}$) of rate predictions being excluded. The astrophysical implications of the GW150914 detection and these inferred rates are further discussed in [Abbott et al. \(2016b\)](#).

The results presented here depend on assumptions about the masses, spins and cosmological distribution of sources. As GW detectors acquire additional data and their sensitivities improve, we will be able to test these assumptions and deepen our understanding of BBH formation and evolution in the Universe.

2. RATE INFERENCE

A rate estimate requires counting the number of signals in an experiment and then estimating the sensitivity to a population of sources to transform the count into an astrophysical rate. Individually, the count of signals and the sensitivity will depend on specific detection thresholds imposed by the pipeline, but the estimated rates should not depend strongly on such thresholds. We consider various methods of counting signals and employ two distinct search pipelines and obtain a range of broadly consistent rate estimates.

2.1. Counting Signals

Two independent pipelines searched the coincident data for signals matching a compact binary coalescence (CBC) ([Abbott et al. 2016d](#)), each producing a set of coincident search triggers. Both the pycbc pipeline ([Usman et al. 2015](#)) and the gstlal pipeline ([gstlal 2016](#)) perform matched-filter searches for CBC signals using aligned-spin templates ([Taracchini et al. 2014](#); [Pürrer 2015](#)) when searching the BBH parts of the CBC parameter space.

In these searches, single-detector triggers are recorded at maxima of the signal-to-noise ratio (SNR) time series for each template ([Allen et al. 2012](#)); coincident search triggers are formed when pairs of triggers, one from each detector, occur in the same template with a time difference of $\pm 15\text{ ms}$ or less. In the pycbc pipeline, the single-detector SNR is re-weighted by a chi-squared factor ([Allen 2005](#)) to account for template-data mismatch ([Babak et al. 2013](#)); the re-weighted single-detector SNRs are combined in quadrature to produce a detection statistic for search triggers. The gstlal pipeline’s detection statistic, however, is based on a likelihood ratio ([Cannon et al. 2013, 2015](#)) constructed from the single-detector SNRs and a signal-consistency statistic formed by comparing the observed SNR time series with that expected from a signal. An analytic estimate of the distribution of astrophysical signals in multiple-detector SNR and signal consistency statistic space is compared to a measured distribution of single-detector triggers without a coincident counterpart in the other detector to form a multiple-detector likelihood ratio.

The [Farr et al. \(2015\)](#) framework considers two classes of triggers: those whose origin is astrophysical and those whose origin is terrestrial. Terrestrial triggers are the result of either instrumental or environmental effects in the detector. The two types of sources produce triggers with different densities in the space of detection statistics, which we denote as x . Triggers appear in a Poisson process with number density in detection space

$$\frac{dN}{dx} = \Lambda_1 p_1(x) + \Lambda_0 p_0(x), \quad (1)$$

where the subscripts “1” and “0” refer to the astrophysical and terrestrial origin, Λ_1 and Λ_0 are the Poisson mean numbers of triggers of astrophysical and terrestrial type, and p_1 and p_0 are the (normalised) density of triggers of astrophysical and terrestrial origin over detection space. In particular, Λ_1 is the mean number of signals of astrophysical origin above the chosen threshold; it is not the mean number of signals confidently detected (see Section 4). The likelihood for a trigger set with detection statistics $\{x_j | j = 1, \dots, M\}$ is ([Farr et al. 2015](#))

$$\begin{aligned} & \mathcal{L}(\{x_j | j = 1, \dots, M\} | \Lambda_1, \Lambda_0) \\ &= \left\{ \prod_{j=1}^M [\Lambda_1 p_1(x_j) + \Lambda_0 p_0(x_j)] \right\} \exp[-\Lambda_1 - \Lambda_0]. \quad (2) \end{aligned}$$

The gstlal pipeline natively determines the functions $p_0(x)$ and $p_1(x)$ for its detection statistic x (the logarithm of the likelihood ratio). For this analysis a threshold of $x_{\min} = 5$ was applied, which is sufficiently low that the trigger density is dominated by terrestrial triggers near threshold. There were $M = 15848$ triggers observed above this threshold.

For `pycbc`, the quantity x' is the re-weighted SNR detection statistic. (When quoting pipeline-specific values we distinguish `pycbc` quantities with a prime.) We assume that the density of astrophysical triggers follows a histogram of the recovered triggers from the injection sets described in Section 2.2. This properly accounts for the interaction of the various single- and double-interferometer thresholds in the `pycbc` search (Abbott et al. 2016d). At high SNR, where these thresholds are irrelevant, the triggers follow an approximately flat-space volumetric density of

$$p_1(x') \simeq \frac{3x_{\min}'^3}{x'^4}, \quad (3)$$

but they deviate from this at smaller SNR. We estimate p_0 for `pycbc` using known background triggers originating from time-shifted analysis of the single-detector data streams as described in Abbott et al. (2016d). The estimated astrophysical and terrestrial trigger densities for `pycbc` are plotted in Figure 1. We choose a threshold detection statistic, $x'_{\min} = 8$, that is sufficiently small that the trigger density is dominated by the terrestrial triggers near threshold, and select triggers from a subset of the search parameter space (i.e. our bank of template waveforms) which contains GW150914 as well as the mass range considered for possible alternative populations of BBH binaries in Section 3. There are $M' = 270$ two-detector coincident triggers in this range with x' above $x'_{\min} = 8$ in the `pycbc` search (Abbott et al. 2016d).

The thresholds applied to the `pycbc` and `gstlal` triggers for this analysis are *not* equivalent to each other in terms of either SNR or false alarm rate; instead, both thresholds have been chosen so that the rate of triggers of terrestrial origin ($\Lambda_0 p_0$) dominates near threshold.

We impose a prior that is Poisson–Jeffreys for the counts:

$$p(\Lambda_1, \Lambda_0) \propto \frac{1}{\sqrt{\Lambda_1}} \frac{1}{\sqrt{\Lambda_0}}. \quad (4)$$

The posterior on counts is proportional to the product of the likelihood from Eq. (2) and the prior from Eq. (4):

$$p(\Lambda_1, \Lambda_0 | \{x_j | j = 1, \dots, M\}) \propto \left\{ \prod_{j=1}^M [\Lambda_1 p_1(x_j) + \Lambda_0 p_0(x_j)] \right\} \times \exp[-\Lambda_1 - \Lambda_0] \frac{1}{\sqrt{\Lambda_1 \Lambda_0}}. \quad (5)$$

We use the Stan and `emcee` Markov-Chain Monte Carlo samplers (Foreman-Mackey et al. 2013; Stan Development Team 2015b,a) to draw samples from the posterior in Eq. (5) for the two pipelines. For the `pycbc` set above the threshold of $x'_{\min} = 8$, we find the posterior median and 90% credible range $\Lambda_1 = 3.2_{-2.4}^{+4.9}$. For the `gstlal` set above the threshold of $x_{\min} = 5$ we find the

posterior median and 90% credible range $\Lambda_1 = 4.8_{-3.8}^{+7.9}$. Though we have only one event (GW150914) at exceptionally high significance, and one other at marginal significance (LVT151012), the counting analysis shows these to be consistent with the possible presence of several more events of astrophysical origin at lower detection statistic in both pipelines.

Using the posterior on the counts of triggers of astrophysical and terrestrial origin from this analysis, we can compute the posterior probability that each particular coincident event comes from an astrophysical versus terrestrial source. The conditional probability that an event at detection statistic x comes from an astrophysical source is given by (Farr et al. 2015)

$$P_1(x | \Lambda_0, \Lambda_1) = \frac{\Lambda_1 p_1(x)}{\Lambda_1 p_1(x) + \Lambda_0 p_0(x)}. \quad (6)$$

Marginalizing over the posterior for the counts gives

$$P_1(x | \{x_j | j = 1, \dots, M\}) \equiv \int d\Lambda_0 d\Lambda_1 P_1(x | \Lambda_0, \Lambda_1) \times p(\Lambda_1, \Lambda_0 | \{x_j | j = 1, \dots, M\}), \quad (7)$$

which is the posterior probability that an event at detection statistic x is astrophysical in origin given the observed event set (and associated count inference). This probability is displayed for both pipelines in Figure 2. In particular, we calculate the posterior probability that LVT151012 is of astrophysical origin to be 0.84 with the `gstlal` pipeline and 0.91 with the `pycbc` pipeline. These relatively high probabilities, while not high enough to claim LVT151012 as a second detection, are large enough to motivate exploring a second class of BBHs in the Kim et al. (2003) prescription. Both pipelines estimate small FAP values for LVT151012 that are consistent with our high P_1 values; the FAP considers only the terrestrial noise distribution, however, while our analysis considers both astrophysical and terrestrial event distributions, which differ between the pipelines.

Under the assumption that GW150914 and LVT151012 are astrophysical, posterior distributions for system parameters can be derived (Veitch et al. 2015). Both triggers are consistent with BBH merger sources with masses $(m_1, m_2) = (36_{-4}^{+5}, 29_{-4}^{+4}) M_{\odot}$ at redshift $0.09_{-0.04}^{+0.03}$ (GW150914) and $(m_1, m_2) = (23_{-5}^{+18}, 13_{-5}^{+4}) M_{\odot}$ at redshift $0.2_{-0.1}^{+0.1}$ (LVT151012) (Abbott et al. 2016e,d). These numbers are the posterior median and 90% credible range. In the two-dimensional m_1 – m_2 plane the posterior distributions for the two events do not overlap at the 99% credible level; thus, following Kim et al. (2003), we should consider the second event, if astrophysical, to be a separate class of BBH from GW150914.

We extend the analysis described above by assum-

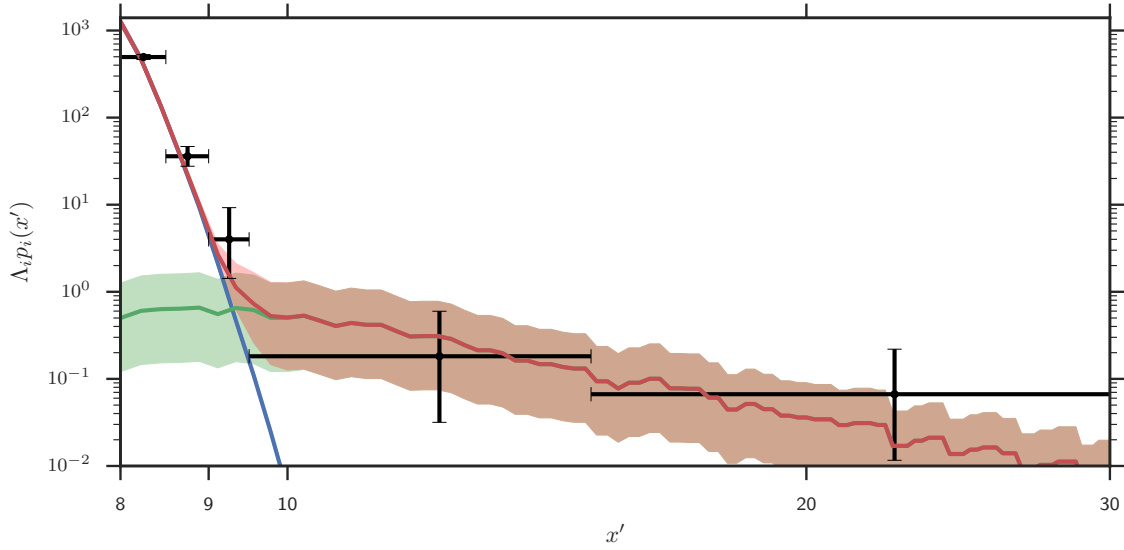


Figure 1. The inferred number density of astrophysical (green), terrestrial (blue), and all (red) triggers as a function of x' for the `pycbc` search (cf. Eq. (1)), using the models for each population described in Section 2.1. The solid lines give the posterior median and the shaded regions give the symmetric 90% credible interval from the posterior in Eq. (5). We also show a binned estimate of the trigger number density from the search (black); bars indicate the 68% confidence Poisson uncertainty on the number of triggers in the y -direction and bin width in the x -direction.

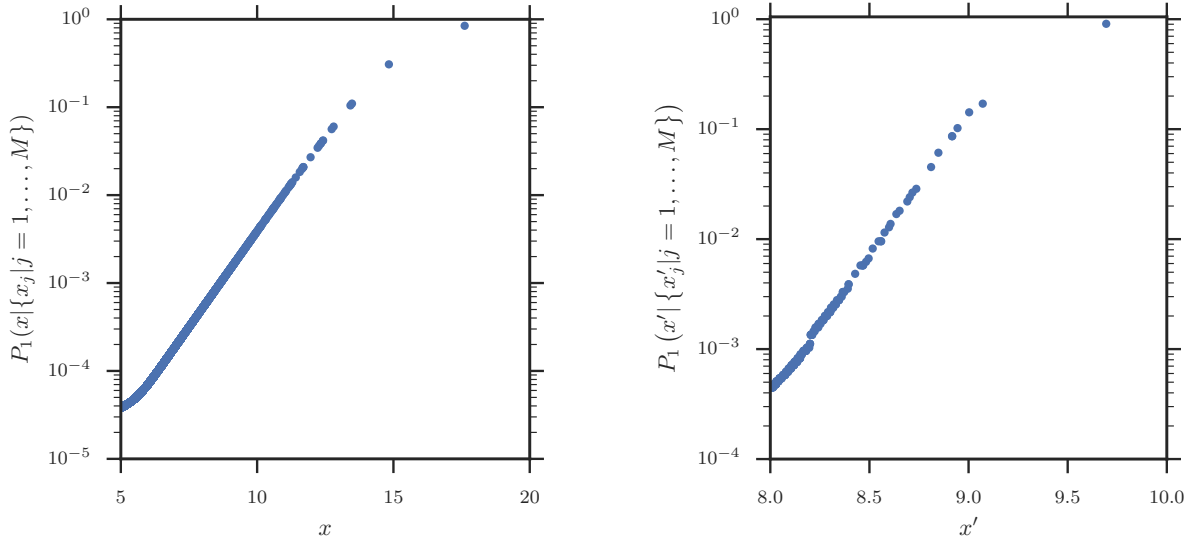


Figure 2. The posterior probability that coincident triggers in our analysis come from an astrophysical source (see Eq. (7)), taking into account the astrophysical and terrestrial counts estimated in section 2.1. Left: the `gstlal` triggers with $x > 5$; right: `pycbc` triggers with $x' > 8$. GW150914 is not shown in the plot because its probability of astrophysical origin is effectively 100%. The only two triggers with $P_1 \gtrsim 50\%$ are GW150914 and LVT151012. For GW150914, we find $P_1 = 1$ to very high precision; for LVT151012, the `gstlal` pipeline finds $P_1 = 0.84$ and the `pycbc` pipeline finds $P_1 = 0.91$.

ing *two* classes of BBH mergers: type 1, which are GW150914-like and type 2, which are LVT151012-like. Our trigger set then consists of triggers of type 1, triggers of type 2, and triggers of terrestrial origin, denoted as type 0. The distribution of triggers over detection statistic, x , now follows an inhomogeneous Poisson process with three terms:

$$\frac{dN}{dx} = \Lambda_1 p_1(x) + \Lambda_2 p_2(x) + \Lambda_0 p_0(x), \quad (8)$$

where Λ_1 , Λ_2 , and Λ_0 are the mean number of triggers of each type in the data set, and p_1 , p_2 , and p_0 are the probability densities for triggers of each type over the detection statistic. The shape of the distribution of SNRs is independent of the event properties, so $p_1 = p_2$; we cannot distinguish BBH classes based only on their trigger distributions, but rather require PE.¹

When an event's parameters are known to come from a certain class i , under the astrophysical origin assumption, then the rate becomes

$$\frac{dN_i}{dx} = \Lambda_i p_i(x) + \Lambda_0 p_0(x), \quad (9)$$

i.e. we permit the event to belong to either its astrophysical class or to an terrestrial source, but not to the other astrophysical class.² The Poisson likelihood for the set of M triggers, $\{x_j | j = 1, \dots, M\}$, exceeding our detection statistic threshold is similar to Eq. (2), but we now account for the distinct classification of GW150914 and LVT151012 based on PE:

$$\begin{aligned} \mathcal{L}(\{x_j | j = 1, \dots, M\} | \Lambda_1, \Lambda_2, \Lambda_0) &= [\Lambda_1 p_1(x_1) + \Lambda_0 p_0(x_1)] [\Lambda_2 p_2(x_2) + \Lambda_0 p_0(x_2)] \\ &\times \left\{ \prod_{j=3}^M [\Lambda_1 p_1(x_j) + \Lambda_2 p_2(x_j) + \Lambda_0 p_0(x_j)] \right\} \\ &\times \exp[-\Lambda_1 - \Lambda_2 - \Lambda_0]. \quad (10) \end{aligned}$$

The first two terms in this product are the rates of the form of Eq. (9) for the GW150914 and LVT151012 triggers, whose class, if not terrestrial, is known; the remain-

¹ In fact, the parameters of the waveform template that produced the trigger can be used to guess at the parameters of the source that generated that trigger, but the bias and uncertainty in this estimate are very large. We therefore ignore the parameters of the waveform template that generated the trigger in the assignment of triggers to BBH classes.

² Strictly speaking, the fact that we have performed PE means that we have examined the full interferometer data surrounding GW150914 and LVT151012, so we should modify the background density: p_0 for these triggers should be the density of terrestrial triggers near the corresponding x that can produce data giving the associated PE posteriors, and p_i should be the density of astrophysical triggers near the corresponding x that can produce data giving the associated PE posteriors. This will modify the density ratio p_i/p_0 , and therefore adjust the probability that LVT151012 is of astrophysical origin; the probability of astrophysical origin for GW150914 will remain 1 to an excellent approximation. This approach to rate estimation is under active development and results will appear in the future.

ing terms in the product over coincident triggers represent the other events, whose class is not known.

We impose a prior that is Poisson–Jeffreys for the total astrophysical and terrestrial counts:

$$p(\Lambda_1, \Lambda_2, \Lambda_0) \propto \frac{1}{\sqrt{\Lambda_1 + \Lambda_2}} \frac{1}{\sqrt{\Lambda_0}} \quad (11)$$

The posterior on counts given the trigger set is proportional to the product of likelihood, Eq. (10), and prior, Eq. (11):

$$\begin{aligned} p(\Lambda_1, \Lambda_2, \Lambda_0 | \{x_j\}) &\propto \mathcal{L}(\{x_j\} | \Lambda_1, \Lambda_2, \Lambda_0) p(\Lambda_1, \Lambda_2, \Lambda_0) \quad (12) \end{aligned}$$

We again use the Stan and `emcee` Markov-Chain Monte Carlo samplers to draw samples from the posterior in Eq. (12). The resulting counts for Λ_1 , Λ_2 , and $\Lambda \equiv \Lambda_1 + \Lambda_2$ are given in Table 2. These parameters represent the Poisson mean number of events of type 1 (GW150914-like), type 2 (LVT151012-like), and both types over the observation, above a very low detection statistic threshold; since this threshold is set at a *different* value for each pipeline we do not expect the counts to be the same between pipelines. Each estimate is consistent with one event of astrophysical origin at very high (GW150914) probability, a further trigger with high (LVT151012) probability, and possibly several more of each type in the set of triggers at lower significance. In the next subsection, we will describe how to turn these counts of events into astrophysical rates.

2.2. Rates

The crucial element in the step from counts to rates is to determine the sensitivity of the search. Search sensitivity is described by the selection function, which gives, as a function of source parameters, the probability of detecting that source in the search. Here we assume that events are uniformly distributed in comoving volume and source time, and describe the distribution of the other parameters (masses, spins, orientation angles, etc.—here denoted by θ) for events of type i by a distribution function, $s_i(\theta)$. Under these assumptions, a count Λ_i becomes a rate R_i via the relation

$$R_i = \Lambda_i / \langle VT \rangle \quad (13)$$

where

$$\langle VT \rangle = T \int dz d\theta \frac{dV_c}{dz} \frac{1}{1+z} s_i(\theta) f(z, \theta). \quad (14)$$

Here R_i is the space-time rate density in the comoving frame, $0 \leq f(z, \theta) \leq 1$ is the selection function, T is the total observation time in the observer frame, $V_c(z)$ is the comoving volume contained within a sphere out to

redshift z (Hogg 1999).³ We need to know—or assume— s_i , the population distribution for events of type i , before we can turn counts into rates.

The Kim et al. (2003) assumption is that the population follows the observed sources:

$$s_i(\theta) = \delta(\theta - \theta_i), \quad (15)$$

where δ is the Dirac delta function and θ_i are the parameters of source type i . Because of the finite SNR of the events, we do not know these parameters perfectly; we marginalize over our imperfect knowledge by integrating over the PE posterior for the intrinsic, source-frame parameters from the followup on each trigger. This effectively replaces the Dirac delta in Eq. (15) by the PE posterior distribution in the integral in Eq. (14).

It is possible to obtain a rough estimate of the BBH coalescence rate from only the GW150914 trigger using a high-significance threshold on the FAP, and a correspondingly restrictive selection function to estimate sensitive time-volumes, so that only this one event is above threshold. We impose a nominal one-per-century threshold on the FAR (corresponding to FAP smaller than 4.3×10^{-4} and a pycbc detection statistic $x' \geq 10.1$). The GW150914 trigger is the only one that exceeds this threshold. We estimate the integral in Eq. (13) via a Monte Carlo procedure. We inject SEOBNRv2 waveforms (Taracchini et al. 2014; Pürrer 2015) with source-frame masses and spins sampled from the posterior distributions from the PE of the GW150914 trigger described in Abbott et al. (2016e,d), random orientations and sky locations, and a fixed redshift distribution into our data stream.⁴ The waveforms produced by SEOBNRv2 have black hole (BH) spins aligned with the orbital angular momentum; in nature we would never expect perfect alignment, but nevertheless the SEOBNRv2 waveforms are a good fit to the observed data (Abbott et al. 2016e) and we therefore expect they will accurately represent our true detection efficiency for sources of this type.

We search this modified data stream using the pycbc pipeline and record all injections found above the threshold $x' \geq 10.1$ for inclusion in our trigger sets. By weighting the recovered injections appropriately, we can estimate the integral in Eq. (14), and, accounting for the effect on the recovered luminosity distance from a 10% amplitude calibration uncertainty (Abbott et al. 2016c), we obtain $\langle VT \rangle_{100} = 0.082^{+0.053}_{-0.032} \text{ Gpc}^3 \text{ yr}$. Systematic uncertainties in the waveforms used for the injections and search are estimated to induce an uncertainty in the sensitive volume calculation that is much smaller than the

calibration uncertainty (Aasi et al. 2013; Littenberg et al. 2013). With such a high threshold, any trigger is virtually certain to be astrophysical in origin, so $p_0 \simeq 0$ (see Section 2.1), thus the posterior on the associated rate, R_{100} becomes (we use a Jeffreys prior, $p(R) \propto 1/\sqrt{R}$):

$$p(R_{100} | \text{GW150914}) \propto \sqrt{R_{100} \langle VT \rangle_{100}} \exp[-R_{100} \langle VT \rangle_{100}], \quad (16)$$

from which we infer the posterior median and 90% credible range $R_{100} = 14^{+39}_{-12} \text{ Gpc}^{-3} \text{ yr}^{-1}$.

As discussed in Section 2.1, there is useful information about the merger rate from triggers with FAR less significant than one per century. Following Farr et al. (2015) we set a lower acceptance threshold such that the trigger density at threshold is dominated by triggers of terrestrial origin. As before, we perform a Monte Carlo estimation of the integral in Eq. (14) using posterior distributions from the PE of both the GW150914 and LVT151012 described in Abbott et al. (2016e,d), but with the lower thresholds used in Section 2.1; the results are given in Table 2.

We find that the following approximate, analytic procedure also produces a good approximation to the pycbc Monte-Carlo estimate in Table 2.

1. Generate inspiral–merger–ringdown waveforms in a single detector at various redshifts from the source distribution $s(\theta)$ with random orientations and sky positions.
2. Using the high-sensitivity early Advanced LIGO noise power spectral density from Abbott et al. (2016f), compute the SNR in a single detector.
3. Consider a signal found if the SNR is greater than 8.

Employed with the source distributions described above, this approximate procedure yields $\langle VT \rangle_1 \simeq 0.107 \text{ Gpc}^3 \text{ yr}$ and $\langle VT \rangle_2 \simeq 0.0225 \text{ Gpc}^3 \text{ yr}$ for the sensitivity to the two classes of merging BBH system. Figure 3 shows the sensitive time-volume integrand,

$$\frac{d\langle VT \rangle}{dz} \equiv T \frac{1}{1+z} \frac{dV_c}{dz} \int d\theta s(\theta) f(z, \theta) \quad (17)$$

estimated from this procedure for systems with various parameters superimposed on the Monte-Carlo estimates from the injection campaign described above.

Figure 4 shows the posterior we infer on the rates R_1 , R_2 , and $R \equiv R_1 + R_2$ from our estimates of $\langle VT \rangle_{1,2}$ and the posteriors on the counts from Section 2.1. Results are shown in Table 1 in the rows “GW150914,” “LVT151012,” and “Both.” Because the two pipelines give rate estimates that are in excellent agreement with

³ Throughout this paper, we use the “TT+lowP+lensing+ext” cosmological parameters from Table 4 of Planck Collaboration et al. (2015).

⁴ The source- and observer-frame masses are related by a redshift factor, $(1+z)M^{\text{source}} = M^{\text{observer}}$.

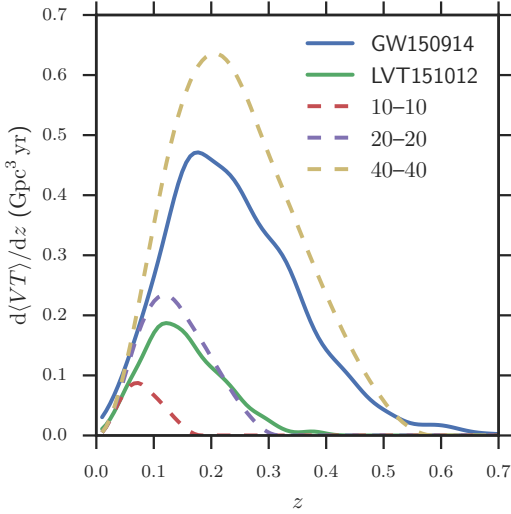


Figure 3. The rate at which sensitive time-volume accumulates with redshift. Curves labeled by component masses in M_{\odot} are computed using the approximate prescription described in Section 2.2, assuming sources with fixed masses in the comoving frame and without spin; the GW150914 and LVT151012 curves are determined from the Monte-Carlo injection campaign described in Section 2.2.

each other, we report a combined rate that gives the median and 90% symmetric credible range for a posterior that is the average of the posterior derived from each pipeline independently. Here, R_1 and R_2 are the contributions to the rate from systems of each class, and R should be interpreted as the total rate of BBH mergers in the local universe.

3. SENSITIVITY TO ASTROPHYSICAL MASS DISTRIBUTION

The assumptions in the Kim et al. (2003) method about the distribution of intrinsic BBH population parameters are strong and almost certainly unrealistic. To test the sensitivity of our rate estimate to the assumptions about BH masses, we report in this section on two additional estimates of the rate using different source distributions $s(\theta)$ that bracket possible astrophysical scenarios. These results are shown in the “Flat” and “Power Law” rows of Table 1

The first source distribution we take to be uniform in aligned spins, $-0.99 \leq (a/m)_{1,2} \leq 0.99$ and flat in $\log(m_1)$ and $\log(m_2)$:

$$s(\theta) \sim \frac{1}{m_1} \frac{1}{m_2}, \quad (18)$$

with $5 M_{\odot} \leq m_1, m_2 \leq 100 M_{\odot}$ and $10 M_{\odot} \leq m_1 + m_2 \leq 100 M_{\odot}$. This distribution likely weights more heavily toward high-mass BHs than the true astrophysical dis-

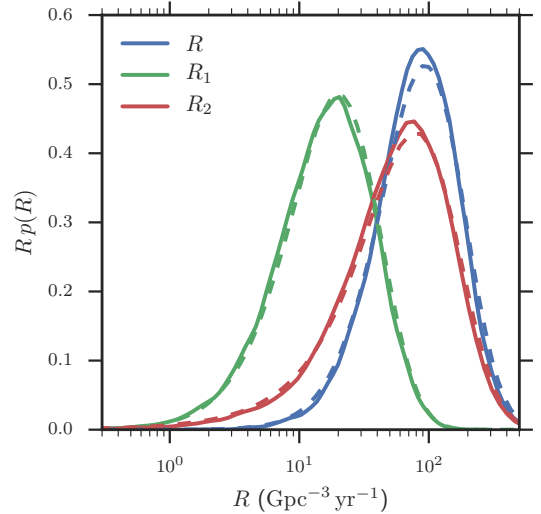


Figure 4. The posterior density on the rate of GW150914-like BBH inspirals, R_1 (green), LVT151012-like BBH inspirals, R_2 (red), and the inferred total rate, $R = R_1 + R_2$ (blue). The median and 90% credible levels are given in Table 1. Solid lines give the rate inferred from the `pycbc` trigger set, while dashed lines give the rate inferred from the `gstlal` trigger set.

tribution (Fryer & Kalogera 2001; Fryer et al. 2012; Dominik et al. 2012; Spera et al. 2015). We choose $5 M_{\odot}$ for the lower mass limit because it encompasses the inferred mass range from PE on LVT151012 and because there are indications of a mass gap between the heaviest neutron stars and the lightest BHs (Özel et al. 2010; Farr et al. 2011); but see Kreidberg et al. (2012) for an alternative explanation for the dearth of BH mass estimates below $\sim 5 M_{\odot}$.

Using an injection campaign as described above, and incorporating calibration errors, we estimate the sensitive time-volume for this population; see Table 2. High-mass BHs from the $5 M_{\odot}$ – $100 M_{\odot}$ range produce high signal-to-noise ratios in the detectors, so this time-volume estimate is likely higher than that for the true astrophysical distribution; the corresponding rate estimate is therefore probably lower than the true BBH rate.

The second source distribution we take to be a power-law on the larger BH mass, following⁵

$$p(m_1) \sim m_1^{-2.35}, \quad (19)$$

with the smaller mass distributed uniformly in $q \equiv$

⁵ The power chosen here is the same as the Salpeter IMF (Salpeter 1955), but this should not be understood to suggest that the distribution of the more massive BH in a binary would follow the IMF; the initial mass–final mass relation for massive stars is complicated and nonlinear (Fryer & Kalogera 2001; Fryer et al. 2012; Dominik et al. 2012; Spera et al. 2015). Instead, as described in the text, this distribution is designed to provide a reasonable lower-limit for the sensitive time-volume and upper limit for the rate.

m_2/m_1 , and with $5 M_\odot \leq m_2 \leq m_1 \leq 100 M_\odot$ and $m_1 + m_2 \leq 100 M_\odot$. Using this distribution in an injection campaign yields the results shown in Table 2. This distribution likely produces more low-mass BHs than the true astrophysical distribution, and therefore the sensitive time-volume is probably smaller than would be obtained with the true distribution; the estimated rate is correspondingly higher.

We use the same astrophysical and terrestrial trigger densities as described in Section 2.1; we now consider all triggers to belong to only two populations, an astrophysical and a terrestrial population, as in the analysis at the beginning of Section 2.1 (see Eq. (5)). We relate counts, Λ_1 , to rates via Eq. (13), with the $\langle VT \rangle$ for the astrophysical distributions given in Table 2. The posteriors on the limiting rates, R_{flat} and R_{pl} , together with the reference BBH coalescence rate R from Section 2 appear in Figure 5. A summary of the various inferred rates appears in Table 1.

4. DISCUSSION

In the absence of clear detections, previous LIGO-Virgo observing runs have yielded merger rate upper limits (Aasi et al. 2013). Even the most optimistic assumptions about the BBH distribution from Section 3 imply rates that are significantly below the corresponding distribution-averaged upper limits from Aasi et al. (2013). For the rate estimates from Section 2.2, the corresponding upper limits from Aasi et al. (2013) are $140 \text{ Gpc}^{-3} \text{ yr}^{-1}$ and $420 \text{ Gpc}^{-3} \text{ yr}^{-1}$; compared to $R_1 = 17_{-13}^{+39} \text{ Gpc}^{-3} \text{ yr}^{-1}$ and $R_2 = 62_{-54}^{+165} \text{ Gpc}^{-3} \text{ yr}^{-1}$, it is clear that the sensitive time-volume reach of Advanced LIGO, even from only 16 days of coincident observations, is vastly larger than that of any previous gravitational-wave observations.

A `pycbc` detection statistic of $x' \geq 10.1$ corresponds to FARs smaller than one per century—an exceptionally significant event. From the signals with $x' \geq 8$ only a fraction 0.49 will have $x' \geq 10.1$. One may wonder, then, how many of these highly significant events we can expect to see in future observations.

For a Poisson mean occurrence number Λ with $x' \geq 8$ in an experiment with sensitive time-volume $\langle VT \rangle_0$, the number of highly significant triggers with FARs smaller than one per century in subsequent experiments with sensitive time-volume $\langle VT \rangle'$ will follow a Poisson distribution with mean

$$\Lambda' = 0.49 \Lambda_1 \frac{\langle VT \rangle'}{\langle VT \rangle_0}. \quad (20)$$

We plot the median value for Λ' obtained in this way, as well as the 90% credible interval, as a function of surveyed time-volume in the left panel of Figure 6. There is, unsurprisingly, a wide range of reasonable possibilities for

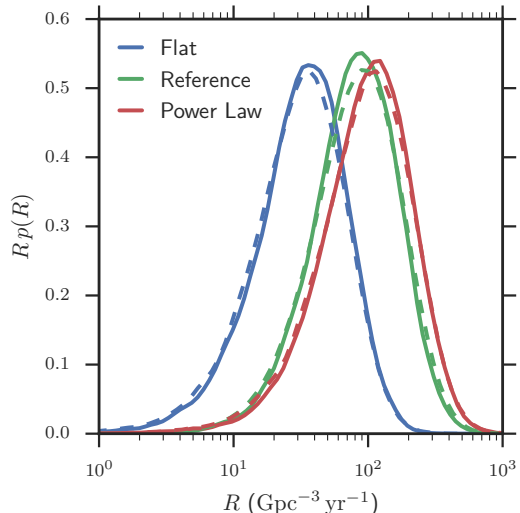


Figure 5. Sensitivity of the inferred BBH coalescence rate to the assumed astrophysical distribution of BBH masses. The curves represent the posterior assuming that BBH masses are flat in $\log(m_1)$ - $\log(m_2)$ (blue; “Flat”), are exactly GW150914-like or LVT151012-like as described in Section 2 (green; “Reference”), or are distributed as in Eq. (19) (red; “Power Law”). The `pycbc` results are shown in solid lines and the `gstlal` results are shown in dotted lines. Though the searches differ in their models of the astrophysical and terrestrial triggers, the rates inferred from each search are very similar. The posterior median rates and symmetric 90% CL intervals are given in Table 1. Comparing to the total rate computed using the assumptions in Kim et al. (2003) in Section 2 we see that the rate can change by a factor of a few depending on the assumed BBH population. In spite of this seemingly-large variation, all three rate posterior distributions are consistent within our statistical uncertainties.

the number of highly significant events in future observations. The 90% credible interval for the expected number of highly significant events is larger than one when $\langle VT \rangle'$ is approximately twice $\langle VT \rangle_0$. The expected number of highly significant events, then, is larger than one at 90% confidence for any experiment surveying approximately twice the time-volume analyzed in this paper. As a point of reference, we show the expected value of $\langle VT \rangle$ for the second and third planned observing runs, O2 and O3. These volumes are calculated as in (Abbott et al. 2016b), for an equal-mass binary with non-spinning components and total mass $60 M_\odot$, assuming an observation of 6 months for O2 and 9 months for O3 with the same coincident duty cycle as during the first 39 d days of O1. We find estimates of $\langle VT \rangle_{\text{O2}} / \langle VT \rangle_0$ between 6.7 and 25.8, and $\langle VT \rangle_{\text{O3}} / \langle VT \rangle_0$ between 29 and 70.

Conditional on the count of loud events, Λ' , we can

Table 2. Counts and sensitive time-volumes to BBH mergers estimated under various assumptions. See Sections 2.1 and 2.2.

	Λ		$\langle VT \rangle / \text{Gpc}^3 \text{ yr}$	
	pycbc	gstlal	pycbc	gstlal
GW150914	$2.1^{+4.1}_{-1.7}$	$3.6^{+6.9}_{-2.9}$	$0.130^{+0.084}_{-0.051}$	$0.21^{+0.14}_{-0.08}$
LVT151012	$2.0^{+4.0}_{-1.7}$	$3.0^{+6.8}_{-2.7}$	$0.032^{+0.020}_{-0.012}$	$0.048^{+0.031}_{-0.019}$
Both	$4.5^{+5.5}_{-3.1}$	$7.4^{+9.2}_{-5.1}$
Astrophysical				
Flat			$0.093^{+0.060}_{-0.036}$	$0.150^{+0.096}_{-0.059}$
Power Law	$3.2^{+4.9}_{-2.4}$	$4.8^{+7.9}_{-3.8}$	$0.031^{+0.020}_{-0.012}$	$0.0479^{+0.031}_{-0.019}$

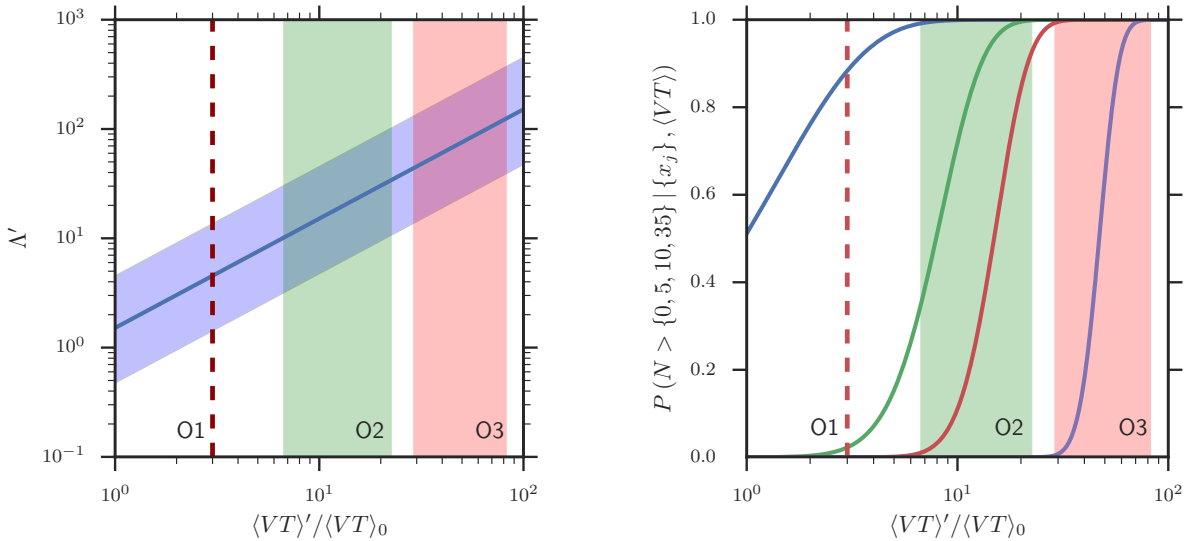


Figure 6. Left panel: The median value and 90% credible interval for the expected number of highly significant events (FARs $< 1/\text{century}$) as a function of surveyed time-volume in an observation (shown as a multiple of $\langle VT \rangle_0$). The expected range of values of $\langle VT \rangle$ for the observations in O2 and O3 are shown as vertical bands. Right panel: The probability of observing $N > 0$ (blue), $N > 5$ (green), $N > 10$ (red), and $N > 35$ (purple) highly significant events, as a function of surveyed time-volume. The vertical line and bands show, from left to right, the expected sensitive time-volume for each of the O1 (dashed line), O2, and O3 observations.

compute the probability of having more than n high-significance events in a subsequent observation:

$$p(N > n | \Lambda') = \exp[-\Lambda'] \sum_{k=n+1}^{\infty} \frac{\Lambda'^k}{k!}. \quad (21)$$

Applying Eq. (20), and integrating over our posterior on Λ from the analysis in Section 2.1, we obtain the posterior probability of more than n high-significance events in a subsequent observation with sensitivity $\langle VT \rangle'$ given our

current observations:

$$p(N > n | \{x_j\}, \langle VT \rangle') = \int d\Lambda_0 d\Lambda_1 p(N > n | \Lambda'(\Lambda_1)) p(\Lambda_0, \Lambda_1 | \{x_j\}). \quad (22)$$

The right panel of Figure 6 shows this probability for various values of n and $\langle VT \rangle'$.

The rates presented here are consistent with the theoretical expectations detailed in [Abadie et al. \(2010\)](#). See [Abbott et al. \(2016b\)](#) for a detailed discussion of the implications of our rate estimates for models of the binary BH population.

GW150914 is unusually significant; only $\sim 8\%$ of the astrophysical distribution of sources with a FAR

smaller than one per century will be more significant than GW150914. However, it is not so significant as to call into question the assumption used here that BBH coalescences are distributed uniformly in comoving volume and source time. As we accumulate more BBH sources with ongoing Advanced LIGO observing runs, we may eventually be able to test this assumption. Similarly, as we accumulate more sources and observation time, we will learn more about the mass distribution of BBH systems. This is only the beginning.

The authors gratefully acknowledge the support of the United States National Science Foundation (NSF) for the construction and operation of the LIGO Laboratory and Advanced LIGO as well as the Science and Technology Facilities Council (STFC) of the United Kingdom, the Max-Planck-Society (MPS), and the State of Niedersachsen/Germany for support of the construction of Advanced LIGO and construction and operation of the GEO600 detector. Additional support for Advanced LIGO was provided by the Australian Research Council. The authors gratefully acknowledge the Italian Istituto Nazionale di Fisica Nucleare (INFN), the French Centre National de la Recherche Scientifique (CNRS) and the Foundation for Fundamental Research on Matter supported by the Netherlands Organisation for Scientific Research, for the construction and operation of the Virgo detector and the creation and support of the EGO consortium. The authors also gratefully acknowledge research support from these agencies as well as by the Council of Scientific and Industrial Research of India, Department of Science and Technology, India, Science & Engineering Research Board (SERB), India, Ministry of Human Resource Development, India, the Spanish Ministerio de Economía y Competitividad, the Conselleria d’Economia i Competitivitat and Conselleria d’Educació, Cultura i Universitats of the Govern de les Illes Balears, the National Science Centre of Poland, the European Commission, the Royal Society, the Scottish Funding Council, the Scottish Universities Physics Alliance, the Hungarian Scientific Research Fund (OTKA), the Lyon Institute of Origins (LIO), the National Research Foundation of Korea, Industry Canada and the Province of Ontario through the Ministry of Economic Development and Innovation, the Natural Science and Engineering Research Council Canada, Canadian Institute for Advanced Research, the Brazilian Ministry of Science, Technology, and Innovation, Russian Foundation for Basic Research, the Leverhulme Trust, the Research Corporation, Ministry of Science and Technology (MOST), Taiwan and the Kavli Foundation. The authors gratefully acknowledge the support of the NSF, STFC, MPS, INFN, CNRS and the State of Niedersachsen/Germany for provision of

computational resources. This article has been assigned the document number [LIGO-P1500217](#).

REFERENCES

- Aasi, J. et al. 2013, *Phys. Rev. D*, 87, 022002, arXiv:1209.6533
- Abadie, J. et al. 2010, *Classical and Quantum Gravity*, 27, 173001, arXiv:1003.2480
- Abbott, B., et al. 2016a, *Phys. Rev. Lett.*, 116, 061102, <https://dcc.ligo.org/LIGO-P150914/public/main>
- . 2016b, *Astrophys. J. Lett.*, 818, 22, <https://dcc.ligo.org/LIGO-P1500262/public/main>
- . 2016c, <https://dcc.ligo.org/LIGO-P1500248/public/main>
- . 2016d, <https://dcc.ligo.org/LIGO-P1500269/public/main>
- . 2016e, <https://dcc.ligo.org/LIGO-P1500218/public/main>
- Abbott, B. P., et al. 2016f, *Living Rev. Relat.*, 19, 1, arXiv:1304.0670
- Allen, B. 2005, *Phys. Rev.*, D71, 062001, arXiv:gr-qc/0405045
- Allen, B., Anderson, W. G., Brady, P. R., Brown, D. A., & Creighton, J. D. E. 2012, *Phys. Rev.*, D85, 122006, arXiv:gr-qc/0509116
- Babak, S., Biswas, R., Brady, P., Brown, D., Cannon, K., et al. 2013, *Phys. Rev.*, D87, 024033, arXiv:1208.3491
- Cannon, K., Hanna, C., & Keppel, D. 2013, *Phys. Rev. D*, 88, 024025, arXiv:1209.0718
- Cannon, K., Hanna, C., & Peoples, J. 2015, ArXiv e-prints, arXiv:1504.04632
- Dominik, M., Belczynski, K., Fryer, C., Holz, D. E., Berti, E., Bulik, T., Mandel, I., & O’Shaughnessy, R. 2012, *ApJ*, 759, 52, arXiv:1202.4901
- Farr, W. M., Gair, J. R., Mandel, I., & Cutler, C. 2015, *Phys. Rev. D*, 91, 023005, arXiv:1302.5341
- Farr, W. M., Sravan, N., Cantrell, A., Kreidberg, L., Bailyn, C. D., Mandel, I., & Kalogera, V. 2011, *ApJ*, 741, 103, arXiv:1011.1459
- Foreman-Mackey, D., Hogg, D. W., Lang, D., & Goodman, J. 2013, *PASP*, 125, 306, arXiv:1202.3665
- Fryer, C. L., Belczynski, K., Wiktorowicz, G., Dominik, M., Kalogera, V., & Holz, D. E. 2012, *ApJ*, 749, 91, arXiv:1110.1726
- Fryer, C. L., & Kalogera, V. 2001, 554, 548, arXiv:astro-ph/9911312
- gstlal. 2016, TBD, TBD, TBD
- Hogg, D. W. 1999, ArXiv Astrophysics e-prints, arXiv:astro-ph/9905116
- Kalogera, V., Belczynski, K., Kim, C., O’Shaughnessy, R., & Willems, B. 2007, *Phys. Rep.*, 442, 75, arXiv:astro-ph/0612144
- Kim, C., Kalogera, V., & Lorimer, D. R. 2003, *ApJ*, 584, 985, arXiv:astro-ph/0207408
- Kreidberg, L., Bailyn, C. D., Farr, W. M., & Kalogera, V. 2012, *ApJ*, 757, 36, arXiv:1205.1805
- Littenberg, T. B., Baker, J. G., Buonanno, A., & Kelly, B. J. 2013, *Phys. Rev. D*, 87, 104003, arXiv:1210.0893
- Özel, F., Psaltis, D., Narayan, R., & McClintock, J. E. 2010, *ApJ*, 725, 1918, arXiv:1006.2834
- Planck Collaboration et al. 2015, ArXiv e-prints, arXiv:1502.01589
- Pürrer, M. 2015, ArXiv e-prints, arXiv:1512.02248
- Salpeter, E. E. 1955, *ApJ*, 121, 161
- Spera, M., Mapelli, M., & Bressan, A. 2015, *MNRAS*, 451, 4086, arXiv:1505.05201
- Stan Development Team. 2015a, PyStan: the Python interface to Stan, Version 2.7.0
- . 2015b, Stan: A C++ Library for Probability and Sampling, Version 2.8.0

Taracchini, A., et al. 2014, Phys. Rev., D89, 061502,
arXiv:1311.2544

Usman, S. A. et al. 2015, ArXiv e-prints, arXiv:1508.02357

Veitch, J. et al. 2015, Phys. Rev. D, 91, 042003, arXiv:1409.7215